Journal of Physics D: Applied Physics

PAPER • **OPEN ACCESS**

RF power transfer efficiency and plasma parameters of low pressure high power ICPs

To cite this article: D Zielke *et al* 2021 *J. Phys. D: Appl. Phys.* **54** 155202

OPEN ACCESS
IOP Publishing
Journal of Physics D: Applied Physics
J. Phys. D: Appl. Phys. **54** (2021) 155202 (9pp)
https://doi.org/10.1088/1361-6463/abd8ee

RF power transfer efficiency and plasma parameters of low pressure high power ICPs

D Zielke[1], S Briefi[1] and U Fantz[1,2]

[1] Max-Planck-Institut für Plasmaphysik, Boltzmannstr. 2, Garching 85748, Germany
[2] AG Experimentelle Plasmaphysik, Universität Augsburg, Augsburg 86135, Germany

E-mail: dominikus.zielke@ipp.mpg.de

Received 5 September 2020, revised 10 November 2020
Accepted for publication 6 January 2021
Published 1 February 2021

Abstract

Inductively coupled radio frequency (RF) ion sources operating at 1 MHz under the condition of a low gas pressure of 0.3 Pa are the basis of negative hydrogen/deuterium ionbased neutral beam injection systems of future fusion devices. The applied high RF powers of up to 75 kW impose considerable strain on the RF system and so the RF power transfer efficiency η becomes a crucial measure of the ion source's reliability. η depends on external parameters such as geometry, RF frequency, power, gas pressure and hydrogen isotope. Hence, η along with the plasma parameters are investigated experimentally at the ITER prototype RF ion source. At only 45%–65% in hydrogen and an increase of around 5% in deuterium, η is found to be surprisingly low in this ion source. The power that is not coupled to the plasma is lost by Joule heating of the RF coil (∼26%) and due to eddy currents in the internal Faraday screen (∼74%). The matching transformer adds up to 8 kW of losses to the system. The low values of η and the high share of the losses in the Faraday screen and the transformer strongly suggest optimization opportunities. At high power densities well above 5 W cm^{-3}, indications for neutral depletion as well as for the ponderomotive effect are found in the pressure and power trends of η and the plasma parameters. The comprehensive data set may serve for comparison with other RF ion sources and more standard inductively coupled plasma setups as well as for validating models to optimize RF coupling.

Keywords: inductively coupled plasma, NNBI, low pressure low temperature plasma, RF power transfer efficiency, Faraday screen, ITER prototype RF ion source, RF power coupling

(Some figures may appear in colour only in the online journal)

1. Introduction

One important application of inductively coupled plasmas (ICPs), among other purposes such as materials processing [1] and space propulsion [2], is as the ion source used in nuclear fusion neutral beam injection systems based on negative hydrogen ions (NNBIs) [3]. An example at a low radio frequency (RF) of 1 MHz, a high generator power of up to 75 kW and a low gas pressure between 0.2 and 0.6 Pa with a focus on 0.3 Pa is the prototype ion source for ITER at the BATMAN Upgrade (BUG) testbed [4, 5]. In this ion source, which is operated in pulsed mode with a maximal pulse length of around 5 s, plasma is generated in a compact, half-closed cylindrical vessel of around 8 l—called the driver—where high electron temperatures around 10 eV and plasma densities around 10^{18} m^{-3} are reached at a gas pressure of 0.3 Pa. The driver's axial length is around 17 cm and its inner radius is around 12 cm, i.e. its low aspect ratio L/R is around 1.4. Its

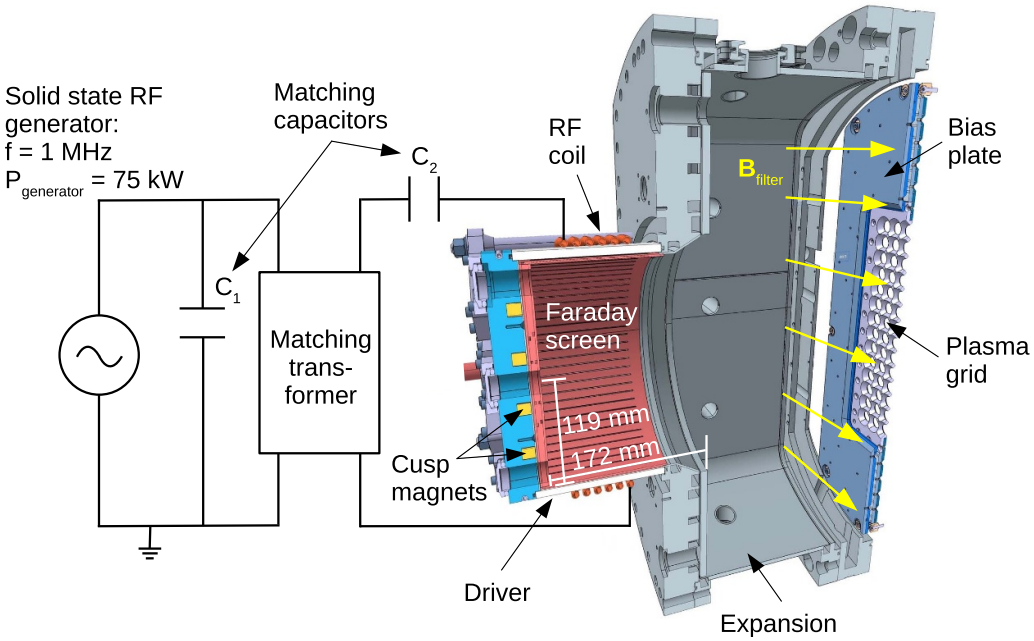

Figure 1. CAD drawing and electrical circuit of the RF ion source of the BATMAN Upgrade testbed. More details about the ion source can be found in [4].

main components are an RF coil with six turns that are wound around a cylindrical dielectric quartz, an internal Faraday screen and a driver backplate. The plasma heating mechanism is purely inductive, since the internal Faraday screen suppresses capacitive coupling and thus protects the quartz against sputtering [6]. The driver backplate is equipped with small permanent magnets that generate a cusp field to increase the plasma density in the driver. The plasma produced in the driver diffuses through the open axial side into a larger expansion region. For further information about the expansion region (inclusive magnetic filter, bias plate and plasma grid), the modular design of NNBI ion sources, H^- production and beam formation, see [4, 5, 7].

At the high generator powers of up to 75 kW used in the BUG ion source, the strain on the RF system is considerable, i.e. electrical breakdowns and arcs become likely, and thus reliable operation of the RF ion source is at risk. Typically, not all of the RF generator power is absorbed by the plasma but only a certain fraction, which is quantified by the RF power transfer efficiency η. The rest of the power is lost by Joule heating of the RF coil, the internal Faraday screen and the surrounding metallic structure, where eddy currents are driven. Note that the definition of η does not include the losses in the RF generator, which is a transistorized radio transmitter from TRANSRADIO SenderSysteme Berlin AG. As stated in [7], its electrical efficiency of around 90% is already high. Hence, further optimization of the RF generator is not in the scope of this work. At the BUG ion source, there is a matching transformer to electrically isolate the ion source of high potential from the grounded RF generator [8]. The nonlinear magnetization losses in its ferrite core decrease η. Moreover, η also depends on external parameters such as the generator power, RF frequency, driver geometry, gas pressure, isotope (hydrogen or deuterium) and on the magnetic filter field (its purpose described in [4]) in a complicated way. Parameter dependency studies would be highly desirable but it is difficult to conduct these with numerical models, since a self-consistent description of the electromagnetic wave generated by the RF coil and the plasma is necessary. First steps in that direction were taken in [9–11], where basic simplified systems were used. However, under the conditions in the driver, i.e. at a low gas pressure of around 0.3 Pa, low RF frequency of 1 MHz and high absorbed power densities well above 5 W cm^{-3}, the heating process is complicated and it is still under active discussion whether the RF skin effect becomes anomalous [9] or even nonlinear [12] in this regime. Effects such as neutral depletion [13] and the ponderomotive force [14] further complicate the attempts to numerically simulate RF coupling in the driver.

A prerequisite for validating such numerical models is an experimental data set of η together with the plasma parameters for a wide range of operating conditions and external parameters, which is obtained in this work. The data set without a matching transformer can also be used to compare the BUG ion source with other RF ion sources and more standard ICP setups. In addition, it is investigated how the losses are distributed among components such as the RF coil, the internal Faraday screen and the matching transformer.

2. Experimental setup and diagnostics

Figure 1 shows an overview of the BUG ion source including RF matching capacitors C_1 and C_2, the matching transformer and the solid-state RF generator.

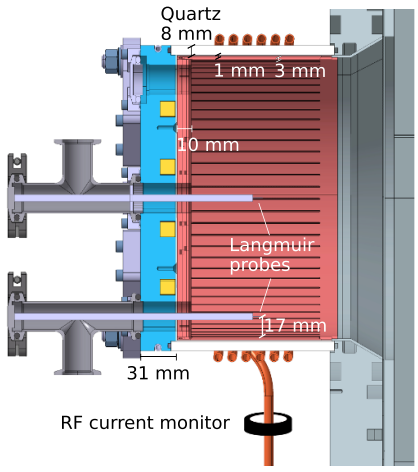

Figure 2. Applied diagnostics at the BUG ion source driver: RF current monitor to determine the amplitude value of the RF coil current I_0 and two Langmuir probes to determine the plasma parameters $\phi_{\text{plasma}}, T_e$ and n_e.

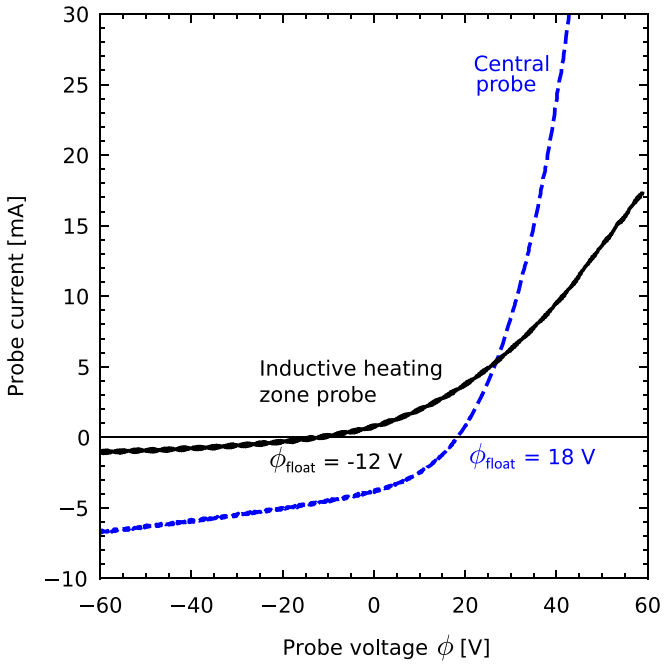

Figure 3. Typical I–V characteristics in the center and in the inductive heating zone with respective floating potentials ϕ_{float}, obtained in hydrogen at $p_{\text{fill}} = 0.5\,\text{Pa}$ and $P_{\text{generator}} = 40\,\text{kW}$.

Under normal beam operating conditions, the matching transformer is used, which adds nonlinear magnetization losses to the system. In pulsed operation mode, its ferrites are air-cooled to ensure that their temperature stays below the Curie temperature of 125 °C. To make the matching transformer ready for longer pulses, different cooling methods depending on the actual losses (assessed in section 3.3.2) have to be considered. To ensure a direct comparison of the results shown in this work with those from other ion sources or more standard ICP setups, all measurements—unless explicitly stated otherwise—were done without the matching transformer.

Specifically for RF power transfer efficiency measurement, the driver is equipped with a current monitor and two Langmuir probes.

The RF current monitor (Pearson model 8537) is installed at the straight feed line part of the RF coil, as indicated in figure 2. It determines the amplitude value of the RF coil current I_0. A subtractive method [15] is used to obtain the RF power transfer efficiency:

$$\eta = \frac{P_{\text{plasma}}}{P_{\text{generator}}} = \frac{P_{\text{generator}} - P_{\text{loss}}}{P_{\text{generator}}}. \tag{1}$$

Herein $P_{\text{generator}} = P_{\text{forward}} - P_{\text{reflected}}$ is the measured generator output power and P_{plasma} is the power that is absorbed by the plasma. $P_{\text{loss}} = \frac{1}{2} R_{\text{network}} I_0^2$ is the power that is lost in the RF network, which comprises the RF coil, the Faraday screen and the surrounding steel structures. The losses associated with it are conveniently quantified by the network resistance R_{network}, which is determined by applying small generator powers $<15\,\text{kW}$ and measuring I_0 while suppressing plasma ignition by keeping the gas inlet valve closed. In this case $P_{\text{loss}} = P_{\text{generator}}$ and the linear relation between P_{loss} and $\frac{1}{2} I_0^2$ determines R_{network}. Note that this method tends to overestimate the loss of power, since the plasma's capability to shield the metallic structure where eddy currents can be driven is not included. However, this overestimation is rather small, because the radial gap between the dielectric and the Faraday screen is only 1 mm, which is around one order of magnitude lower than the RF skin depth, i.e. the damping of the wave there is not effective.

The gas pressure is measured by three capacitive pressure gauges at different positions in the expansion region. During a plasma pulse, the inlet gas flow is provided such that the measured pressure in gas-only operation, i.e. without plasma, is equal to the set pressure. For this reason, the gas pressure is also referred to as filling pressure p_{fill}.

The plasma parameters in the driver, i.e. electron density n_e, plasma potential ϕ_{plasma} and electron temperature T_e, are probed with two Langmuir probes. Both probes are not RF compensated; therefore, special care has to be taken when the obtained I–V characteristics are evaluated, as described later in this section. The probes are axially inserted through the driver backplate, as shown in figure 2. One probe is located in the driver center and the other 17 mm radially away from the inside of the Faraday screen in the vicinity of the RF coil—called the inductive heating zone. Both probe tips are made out of tungsten with lengths and diameters of 5 mm and 50 μm, respectively. Typical I–V characteristics obtained from these probes are depicted in figure 3.

The ion branches of the probes are evaluated using orbital motion limited theory (OML). It was shown by Chen *et al* that this method produces reliable effective ion densities $n_{\text{i,eff}}$, when the probe tip radius is thin compared to the Debye sheath that forms around the probe tip [16, 17]. This is fulfilled for both probes in the driver plasma. For the effective ion mass, a mixture of 20% H_3^+, 40% H_2^+ and 40% H^+ is used, as estimated in [18]. The relative error $\Delta n_{\text{i,eff}}/n_{\text{i,eff}} = 25\%$ is estimated by using different maximum voltages up to which the

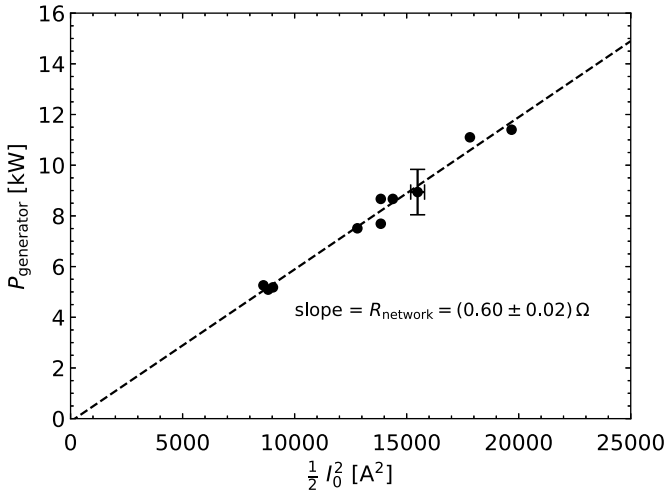

Figure 4. $R_{network}$ is determined from a linear best-fit of $P_{generator}$ over $\frac{1}{2}I_0^2$.

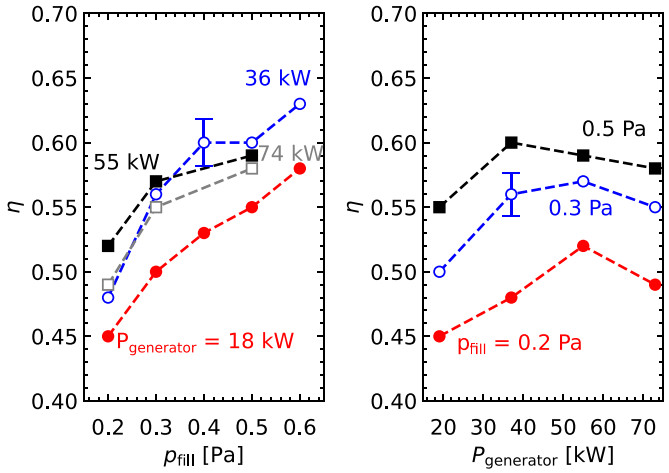

Figure 5. RF power transfer efficiency η in hydrogen for varying p_{fill} and $P_{generator}$.

I–V characteristic are fitted using OML. Quasi-neutrality of the plasma is used to infer the electron density from the effective ion density.

The Langmuir probe analysis of the electron branch is problematic, since the electrons in the inductive heating zone are magnetized by the RF magnetic field. The RF coil can be considered (in a first approximation) cylindrically symmetric and therefore produces a purely axial magnetic field of several mT at the location of the probe tip in the inductive heating zone. Cross-field mobility of electrons onto the probe is strongly impaired, wherefore the electron current remains low even for large applied probe voltages around 60 V, as depicted in figure 3. Therefore, ϕ_{plasma} and T_e cannot be evaluated in the inductive heating zone. However, since there is a skin effect in the plasma, the RF magnetic field is almost absent in the center of the driver; therefore it is possible to access the electron branch of the central probe. As stated earlier, both probes are not RF compensated and therefore the electron branch of the collected probe current data is subject to RF disturbances.

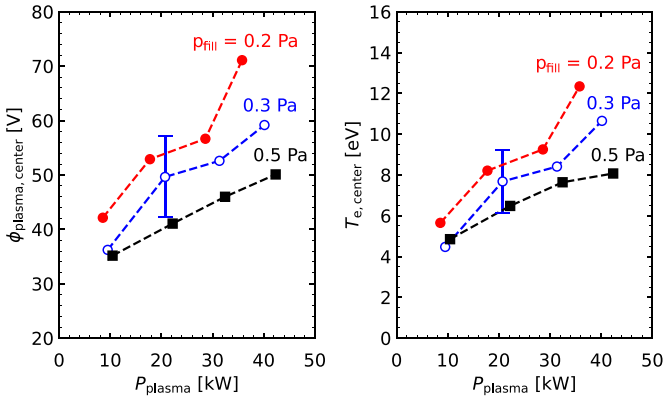

Figure 6. Central ϕ_{plasma} and T_e in hydrogen for varying P_{plasma} at different p_{fill}.

For this reason the standard evaluation method for the electron branch of the I–V characteristics, i.e. probing the electron energy distribution function (EEDF) via the second derivative of the electron current, cannot be used. Instead, an alternative approach, proposed by Chen is employed [19], where the ion current (obtained from OML theory) is subtracted from the total current to obtain the electron current I_e. By assuming I_e to have an EEDF of Maxwell–Boltzmann type that obeys the Boltzmann relation:

$$I_e = A_{probe} n_e e \frac{1}{4} v_{th,e} \exp\left(\frac{V_{probe} - \phi_{plasma}}{eT_e}\right). \quad (2)$$

Herein, A_{probe} denotes the surface of the probe tip, n_e is the electron density (inferred from quasi-neutrality), e is the elementary charge and $v_{th,e} = (8eT_e/\pi m_e)^{1/2}$ is the electron thermal velocity with the electron mass m_e. ϕ_{plasma} and T_e are obtained as independent fitting parameters from a fit with equation (2) up to a voltage well below the floating potential to avoid RF disturbances. The relative errors $\Delta\phi_{plasma}/\phi_{plasma} \approx \Delta T_e/T_e = 20\%$ result again from the used maximum voltage up to which the OML fit is done.

3. Results and discussion

3.1. Network resistance

The Joule losses in the RF coil, the Faraday screen and the surrounding steel structures are quantified by the network resistance $R_{network}$. Following the procedure laid out in section 2, a best-fit of the generator power over $\frac{1}{2}I_0^2$ yields $R_{network} = (0.6 \pm 0.02)\,\Omega$, as shown in figure 4. This value is used in the following section for the evaluation of η.

3.2. Plasma power absorption

As already stated, the plasma's capability to absorb power and thus η depends on external parameters in a complicated way. In the following sections, the impact of the filling pressure, the power absorbed by the plasma, the magnetic filter field and the isotope, i.e. hydrogen or deuterium on η and on the plasma parameters, are investigated.

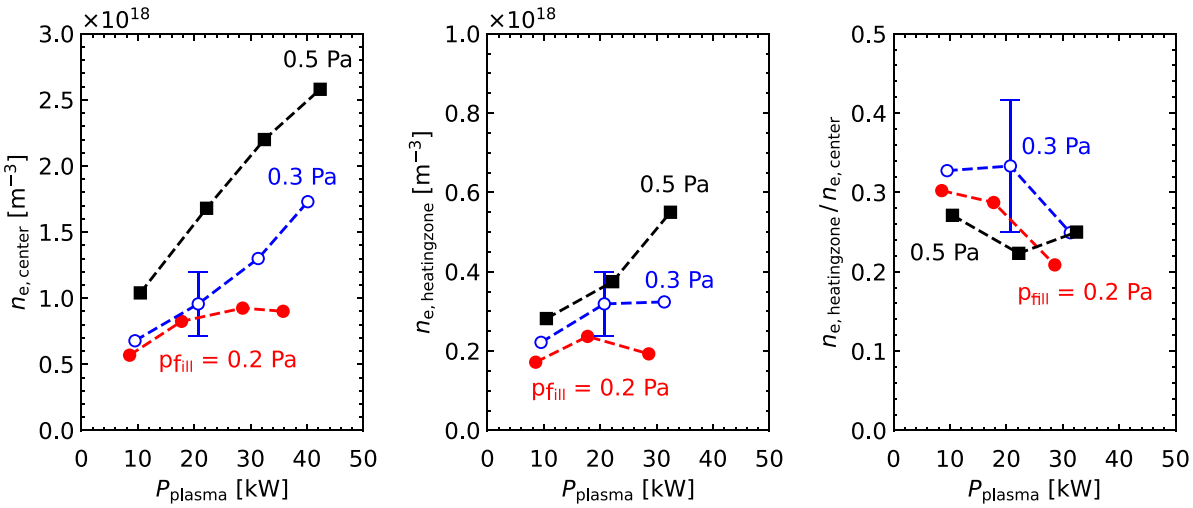

Figure 7. n_e in the driver center and in the inductive heating zone as well as their ratio for varying P_{plasma} at different p_{fill}.

3.2.1. Filling pressure and power variation. Figure 5 shows the RF power transfer efficiency η of the BUG ion source operated in hydrogen for varying filling pressure p_{fill} and generator power $P_{generator}$.

Starting from the highest pressure of 0.6 Pa, η decreases monotonically with decreasing filling pressure for all generator powers. When the generator power is increased, η increases until it reaches a pressure specific maximum value. For further increasing generator powers, η decreases. The generator power at which the maximum η value is obtained is shifted slightly to lower powers for increasing pressure. In general, η is surprisingly low, i.e. only 45%–65% of the generator power is absorbed by the plasma. This means that 35%–55% corresponding to roughly 10–35 kW of the generator power is absorbed by the RF coil, the Faraday screen or by the surrounding steel structures; therefore water cooling of these components is necessary. As these losses change with pressure and power, the plasma parameters are related to P_{plasma} instead of $P_{generator}$ in the following.

Global models [1] can be used to gain a first insight into the underlying physics. When applying these models, one has to be aware that considerable simplifications are used, such as the assumption of a Maxwell–Boltzmann velocity distribution function for all particle species, no spatial variation, a simplified plasma sheath and the neglect of external magnetic fields. Nevertheless, as is shown below, these models can explain some of the locally measured plasma parameter trends.

Figure 6 shows the change of the central plasma potential and electron temperature for varying plasma power at different filling pressures. For a fixed P_{plasma}, ϕ_{plasma} and T_e increase when the pressure is decreased. This can be explained by a simple global model, where the electron particle and energy balance decouple when a stationary neutral particle background is assumed. From the particle balance follows then that T_e increases when the pressure decreases. This is because at lower pressures the electrons gain more energy from the applied external field due to their increased mean free path. However, the increase of T_e with P_{plasma} is not expected from this model. This confirms the high relevance of the correct description of the neutral gas dynamics to capture neutral depletion at these low pressures, as emphasized in [13, 20].

Figure 7 shows the corresponding electron densities in the center, in the inductive heating zone and their ratio. For a fixed P_{plasma}, the increase of n_e with increasing pressure can be explained by the simple global model power balance, where the total power absorbed must equal the total power lost:

$$P_{plasma} = e A_{eff} n_e u_{Bohm}(T_e) \mathcal{E}_{total}(T_e). \quad (3)$$

e is the elementary charge and A_{eff} a constant effective surface area for charged particle losses. The Bohm velocity u_{Bohm} and the total energy lost per electron–ion pair $\mathcal{E}_{total}$ both increase with increasing T_e. Hence, for a fixed P_{plasma}, n_e must increase, when T_e decreases, i.e. when p_{fill} increases. From the simple global model power balance it also follows that n_e should linearly increase with increasing P_{plasma} for a fixed pressure. This is fulfilled for $p_{fill} \geqslant 0.3$ Pa within the error bars. However, for $p_{fill} = 0.2$ Pa, $n_{e,center}$ saturates and $n_{e,heatingzone}$ even slightly decreases for $P_{plasma} \geqslant 20$ kW. This is another indication of the neutral depletion through ionization that is predominant at low filling pressures and high powers [13]. The ratio $n_{e,heatingzone}/n_{e,center}$, ranges between 0.22 and 0.34 and is therefore slightly higher than the value obtained by a simple diffusion model [1], where the resulting Bessel profile yields a ratio of 0.19. This higher ratio is probably caused by the ponderomotive force, that changes the plasma potential and the electron density profile, as is shown in [14, 21]. Also, the magnetic cusp field might play an important role in forming the electron density profile in the driver.

The discussion of the plasma parameter variations above shows that some of the observed trends can be explained quite easily by a simple analytic global model [22]. A complication is introduced when the neutrals are depleted at low pressures but this can still be handled semi-analytically, as shown

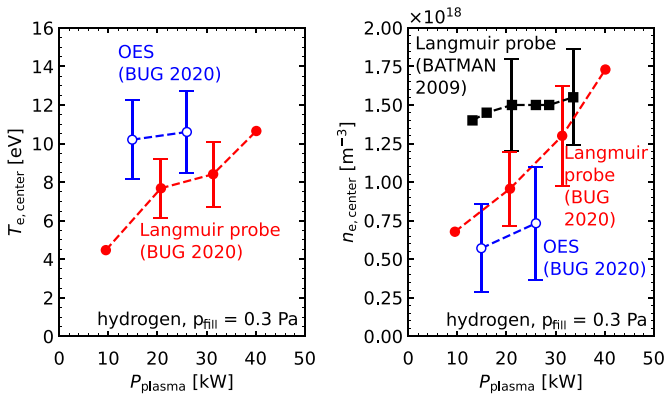

Figure 8. Comparison with OES measurements at the BUG ion source driver [23] and with Langmuir probe measurements at the former BATMAN setup of 2009 [18].

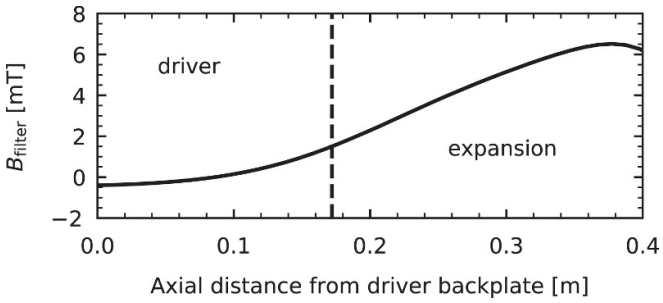

Figure 9. Simulated magnetic filter field B_{filter} along the central driver axis for the maximum plasma grid current of 3 kA. The direction of B_{filter} is indicated in figure 1.

in [13]. However, for understanding how the electrical quantities such as the RF coil current I_0 and η behave when external parameters are changed, it is necessary to describe the plasma and the RF fields self-consistently, involving the right heating regime. In a self-consistent model, it is also possible to include the nonlinear ponderomotive effect and its impact on the spatial profiles of the plasma parameters and on the RF fields in the plasma. Only then one can e.g. explain why η decreases at high RF powers for all pressures, as shown in figure 5, while n_{e} keeps increasing for higher pressures and saturates for lower pressures, as shown in figure 7.

3.2.2. Comparison with results from other diagnostics. Averaged plasma parameters along the central axis through the driver were determined in an earlier campaign by means of optical emission spectroscopy (OES) [23] and are shown here for comparison in figure 8. The obtained electron temperatures and densities fit within error bars to the ones obtained in the present campaign. The electron density determined from the Langmuir probe is slightly higher than the one measured by OES. This is because the OES measurement is line-of-sight-averaged, i.e. the axial profile through the driver and the expansion is accounted for, where it is known from OES measurements in the expansion region, that n_{e} is decreased there [23]. The electron density in the driver has also been measured by Langmuir probes during a previous BUG experiment [18]. In the former experimental setup, aspects such as source geometry, grid system, matching transformer and RF generator were different from the present one, as described in [18]. For a comparison of the electron densities, η from the present setup (including matching transformer losses) is used to estimate P_{plasma} for the former setup. The measured electron densities are in the same range and also the trends are similar, even though the increase of n_{e} with P_{plasma} is more pronounced at the present setup, as shown in figure 8.

3.2.3. Magnetic filter field variation. Various magnetic fields are present in the ion source: (i) checkerboard oriented permanent magnets in the driver backplate (see figure 1 and [4]) generate a cusp magnetic field to increase the plasma density in the driver. In the inductive heating zone, its strength is around 1 mT. (ii) A time-dependent RF magnetic field is caused by the RF coil current. Since in typical operating conditions of the ion source the RF current amplitude is well above 300 A, this results in effective magnetic field strengths in the inductive heating zone of around 10 mT. (iii) A steady-state current that can be varied from 0 to 3 kA through the plasma grid creates a static magnetic filter field B_{filter} of up to 6 mT directly in front of the plasma grid, as shown in figure 1. Its purpose is to cool down the electrons there to reduce the H^- losses caused by electron stripping. The field strength in each point in the discharge is linearly related to the strength of the current through the plasma grid. As can be seen from figure 9, its strength in the driver is smaller than 0.5 mT. Note that the direction of the filter field in the driver is reversed because of the return conductors, which are located outside of the expansion chamber directly behind the conjunction of the driver and the expansion chamber.

Comparing the magnitudes of the different magnetic fields yields that in the driver the RF magnetic field (10 mT) dominates the magnetic filter field (0.5 mT) as well as the cusp magnetic field (1 mT). Consequently, n_{e} and η are almost not affected by the magnetic filter field. However, slight increases of ϕ_{plasma} and T_{e} of around 10 V and 3 eV, respectively, are observed when B_{filter} is increased from 0 to its maximum value of 0.5 mT in the driver (corresponding to a plasma grid current of 3 kA). This can be explained by the heat flux transport barrier that is created by the magnetic filter, which causes T_{e} to drop in the vicinity of the plasma grid but at the same time increases T_{e} in the driver, as shown by Lishev *et al* via fluid modeling of the ion source [10].

3.2.4. Comparison of hydrogen and deuterium. Since ion sources in future fusion devices will operate in deuterium rather than in hydrogen, η in hydrogen and in deuterium are compared in figure 11. η exhibits the same pressure and power trends in H_2 and in D_2. However, it is systematically increased in deuterium by around 5% reaching values just above 60% at 75 kW generator power. For the same P_{plasma}, the electron density is systematically higher in deuterium by a factor of about 1.5, as shown in figure 10. The larger n_{e} in deuterium can be explained by the larger ion masses of deuterium, which

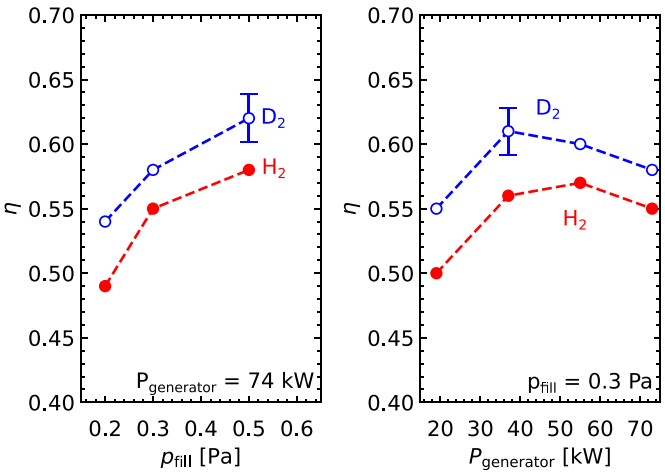

Figure 10. n_e in deuterium and in hydrogen for varying P_{plasma}.

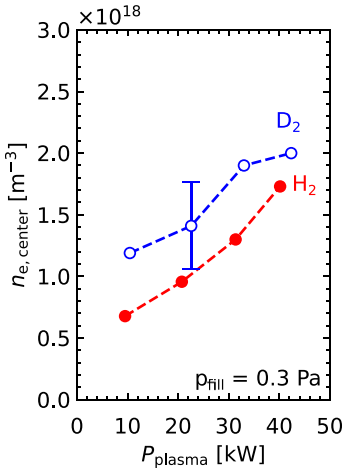

Figure 11. η in deuterium and in hydrogen for varying p_{fill} and $P_{generator}$.

yield smaller mobilities and diffusion coefficients in the ion particle balances. This in turn allows for larger steady-state plasma densities in deuterium compared to hydrogen. Neither ϕ_{plasma} nor T_e are affected by the used isotope within error bars. This surprising fact was also seen in laboratory scale experiments at lower powers [24].

3.3. Losses in ion source components

As shown in section 3.2, a substantial part of the generator power is lost to Joule heating of the ion source components. To identify the exact parts, a 1:1 size mock-up made of spare parts from the BUG ion source driver has been built, where each individual component such as the cylindrical quartz vessel, the RF coil antenna, the driver and source backplates, and the Faraday screen can be mounted separately.

3.3.1. Losses in the RF coil, Faraday screen and backplates. To make sure that the results from the mock-up can be transferred to the BUG setup, the mock-up is assembled in a first step including all potential major RF loss components mentioned above. The internal Faraday screen used in the mock-up (and also in the BUG ion source) has a particular structure, i.e. it consists of a slitted cylinder and a backplate at one side, as shown in figure 2. It is made out of copper and its inner surfaces are coated with a thin molybdenum layer to protect the ion source from sputtering. The resulting $R_{network} = (0.7 \pm 0.02)\,\Omega$ at the mock-up is around 15% larger than $R_{network} = (0.6 \pm 0.02)\,\Omega$ at the BUG ion source driver. The increased $R_{network}$ at the mock-up can be attributed to the different RF coil with seven instead of six turns, which was the only one available as a spare part when the mock-up was built. This yields a smaller distance between the outermost coil turn and the ends of the Faraday screen slits allowing for more eddy currents to be driven there.

Removing the driver and source backplates has no impact on $R_{network}$. From this it can be concluded that the influence of these two components on the network resistance and thus on the network losses is negligible. However, when also the Faraday screen is removed, i.e. when only the RF coil and the quartz cylinder are present, $R_{network}$ and the inductance of the system change so drastically that the RF matching procedure, as described in [1], fails within the experimental limitations. Therefore, $R_{network}$ cannot be evaluated for the coil-only configuration with this method. Instead, a precision LCR meter (Agilent Technologies model E4980A) is used to measure the RF resistance of the coil. At 1 MHz, it is $(0.18 \pm 0.04)\,\Omega$. From this it follows that around $0.18/0.7 \approx 26\%$ of the network losses can be attributed to the RF coil. The rest, i.e. around 74%, have to be absorbed by the Faraday screen.

3.3.2. Losses in the matching transformer. Attached to the BUG ion source is a matching transformer to electrically isolate the ion source at high potential from the grounded RF generator [4, 8]. It has a ferrite core to couple the magnetic fluxes, which is subject to magnetization losses. These are quantified in a generator power sweep at $p_{fill} = 0.3$ Pa with and without a transformer. When operating the source with the matching transformer, different matching capacities have to be used to adjust the load as seen by the RF generator to 50 Ω, because only then is no reflected power oscillating in the system. However, since the power absorbed by these matching capacities is negligible, this has no impact on η. As shown in figure 12, η is decreased when the transformer is used by around 15% for generator powers below 55 kW and by around 10% at high powers around 75 kW. In absolute values, this means that the loss power in the matching transformer increases from around 3 kW at low powers to around 8 kW at high powers. This has to be taken into account for the design of an appropriate cooling system when steady-state operation is considered. It was checked with Langmuir probe measurements that the power that is absorbed by the plasma is the quantity that ultimately determines the plasma parameters and not the generator power, since the latter comprises all losses including the ones of the matching transformer. This is exemplarily shown for n_e for a varying P_{plasma}

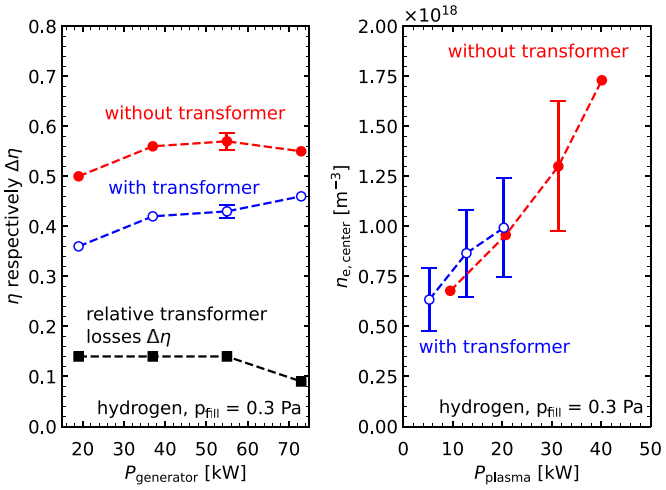

Figure 12. Left: η with and without the transformer for varying $P_{\text{generator}}$. Right: n_e with and without the transformer for varying P_{plasma}.

in figure 12, where the results with and without the transformer agree within measurement error, as expected. This has relevance for comparing the BUG setup, which is by default operated with the matching transformer, with other NNBI ion sources, i.e. $P_{\text{generator}}$ should not be used in such a comparison.

4. Conclusion

For the first time, the RF power transfer efficiency η has been measured at an NNBI ion source under the conditions of low gas pressures of around 0.3 Pa, a low RF frequency of 1 MHz and high RF generator powers of up to 75 kW. Along with η were the plasma parameters in the driver determined by local Langmuir probe measurements for a wide range of operating conditions.

The surprisingly low η ranges between 45% and 65% depended on the operating condition. These values indicate that considerable optimization potential for the plasma to absorb more power corresponding to 10–35 kW is available. Raising this potential would help to reduce the strain on the RF system and the required cooling power. In this way the reliability of the system could be enhanced. The losses are distributed between the Faraday screen and the RF coil, where the former absorbs 74% of the losses through Joule heating by eddy currents and the latter 26% of the losses by direct Joule heating. This indicates that a dedicated optimization of the Faraday screen is worthwhile. All measurements without the BUG-specific matching transformer are directly comparable to other ion sources that do not use a transformer and also to more standard ICP setups, e.g. those used in material processing. It was shown that the quantity that ultimately determines the power trend of the plasma parameters is the power absorbed by the plasma and not the generator power. This has to be considered when plasma parameters of different setups are to be compared. The matching transformer that is used in the BUG normal operating mode adds losses from 3 to 8 kW to the system, which would have to be cooled away in steady-state operating mode.

The discussion of η as well as the spatially localized plasma parameters and their trends with power and pressure showed that to obtain correct dependencies the RF coupling in the driver has to be modeled self-consistently involving the appropriate heating mechanism and phenomena such as neutral depletion and the ponderomotive effect. The comprehensive data set presented in this work can be used for validating a self-consistent model of the RF coupling in the driver, which is currently in preparation.

Acknowledgments

This work was carried out within the framework of the EUROfusion Consortium and has received funding from the Euratom research and training programme 2014–2018 and 2019–2020 under Grant Agreement No. 633053. The views and opinions expressed herein do not necessarily reflect those of the European Commission.

ORCID iDs

D Zielke https://orcid.org/0000-0003-4231-4350
S Briefi https://orcid.org/0000-0003-2997-3503
U Fantz https://orcid.org/0000-0003-2239-3477

References

[1] Lieberman M A *et al* 2005 *Principles of Plasma Discharges and Materials Processing* 2nd edn (New York: Wiley)
[2] Groh K H *et al* 1992 Radio-frequency ion sources for space propulsion *Rev. Sci. Instrum.* **63** 2513
[3] Hemsworth R *et al* 2009 Status of the ITER heating neutral beam system *Nucl. Fusion* **49** 045006
[4] Heinemann B *et al* 2017 Towards large and powerful radio frequency driven negative ion sources for fusion *New J. Phys.* **19** 015001
[5] Heinemann B *et al* 2015 Upgrade of the BATMAN test facility for H^- source development *AIP Conf. Proc.* **1655** 060003
[6] Kraus W *et al* 2012 The development of the radio frequency driven negative ion source for neutral beam injectors *Rev. Sci. Instrum.* **83** 02B104
[7] Kraus W *et al* 2014 Ways to improve the efficiency and reliability of radio frequency driven negative ion sources for fusion *Rev. Sci. Instrum.* **85** 02B309
[8] Gaio E *et al* 2007 Studies on the radio frequency power supply system for the ITER NB injector ion source *Fusion Eng. Des.* **82** 912–19
[9] Hagelaar G J M *et al* 2011 Model of an inductively coupled negative ion source: I. general model description *Plasma Sources Sci. Technol.* **20** 015001
[10] Lishev S *et al* 2015 Spatial distribution of the plasma parameters in the RF negative ion source prototype for fusion *AIP Conf. Proc.* **1655** 040010
[11] Jain P *et al* 2018 Evaluation of power transfer efficiency for a high power inductively coupled radio-frequency hydrogen ion source *Plasma Phys. Control. Fusion* **60** 045007

[12] Froese A M *et al* 2009 Nonlinear skin effect in a collisionless plasma *Phys. Plasmas* **16** 080704
[13] Fruchtman A 2017 Neutral gas depletion in low temperature plasma *J. Phys. D: Appl. Phys.* **50** 473002
[14] Smolyakov A I *et al* 2001 Effect of the electron thermal motion on the ponderomotive force in inductive plasma *Phys. Plasmas* **8** 3857
[15] Hopwood J 1994 Planar RF induction plasma coupling efficiency *Plasma Sources Sci. Technol.* **3** 460
[16] Chen F F 2009 Langmuir probes in RF plasma: surprising validity of OML theory *Plasma Sources Sci. Technol.* **18** 03501
[17] Chen F F *et al* 2012 Calibration of Langmuir probes against microwaves and plasma oscillation probes *Plasma Sources Sci. Technol.* **21** 055002
[18] McNeely P *et al* 2009 A Langmuir probe system for high power RF-driven negative ion sources on high potential *Plasma Sources Sci. Technol.* **18** 014011
[19] Chen F F 2012 Langmuir probe measurements in the intense RF field of a helicon discharge *Plasma Sources Sci. Technol.* **21** 055013
[20] McNeely P *et al* 2011 Neutral depletion in an H^- source operated at high RF power and low input gas flow *Plasma Sources Sci. Technol.* **20** 045005
[21] DiPeso G *et al* 1995 Equilibrium profiles for RF-plasma sources with ponderomotive forces *IEEE Trans. Plasma Sci.* **23** 550–7
[22] Boeuf J P *et al* 2011 Model of an inductively coupled negative ion source: II. application to an ITER type source *Plasma Sources Sci. Technol.* **20** 015002
[23] Briefi S *et al* 2018 Spectroscopic investigations of the ion source at BATMAN Upgrade *AIP Conf. Proc.* **2052** 040005
[24] Rauner D *et al* 2017 RF power transfer efficiency of inductively coupled low pressure H_2 and D_2 discharges *Plasma Sources Sci. Technol.* **26** 095004